Available online at www.sciencedirect.com

ScienceDirect

Nuclear and Particle Physics Proceedings 273–275 (2016) 1807–1813

www.elsevier.com/locate/nppp

Neutrinos and Nuclear Astrophysics at LUNA

Carlo Gustavino

for the LUNA collaboration

INFN Sezione di Roma, I-00185 Roma, Italy

Abstract

Nuclear astrophysics plays an important role in understanding open issues of neutrino physics. As an example, the two key reactions of the solar p-p chain $^3He(^3He, 2p)^4He$ and $^3He(^4He, \gamma)^7Be$ have been studied at low energy with LUNA, providing an accurate experimental footing for the Standard Solar Model and consequently to study the neutrino mixing parameters. The LUNA collaboration is now studying the $D(p, \gamma)^3He$ reaction at Big Bang Nucleosynthesis (BBN) energies. The poor knowledge of this reaction is the main source of the uncertainty of the primordial abundance of deuterium in BBN calculations. In turn, the abundance of deuterium depends on the number of relativistic species existing in the early Universe, making the comparison between observed an calculated abundance of deuterium a powerful tool to constrain the existence of light sterile neutrinos or any other type of *"dark radiation"*.

Keywords: BBN, neutrino, Nuclear astrophysics

1. Nuclear Astrophysics

At energies of interest in astroparticle physics ($0.01 \div 1\ MeV$) the cross-section $\sigma(E)$ drops almost exponentially with decreasing energy E, due to the repulsion of charged nuclei. For this reason, in nuclear astrophysics the nuclear cross section $\sigma(E)$ is often factorized as follows:

$$\sigma(E) = \frac{S(E)e^{-2\pi\eta^*}}{E} \quad (1)$$

In this formula, the exponential term takes into account the Coulomb barrier, while the astrophysical factor $S(E)$ contains all the nuclear effects. For non-resonant reactions, it is a smoothly varying function of energy. The Sommerfeld parameter η^* is given by $2\pi\eta^* = 31.29 Z_1 Z_2 (\mu/E)^{1/2}$. Z_1 and Z_2 are the nuclear charges of the interacting nuclei. μ is their reduced mass (in units of a.m.u.), and E is the center of mass energy (in units of keV).

Due to the low reaction yield, direct measurements at low energy are severely hampered by the background induced by cosmic rays. On the other hand, the extrapolation of the cross section obtained from data at high energy can be wrong because the possible existence of nuclear effects at low energy such as the existence of narrow resonances [1]. For this reason the LUNA collaboration carries out its measurements with the world's only underground accelerator facility, operating at the *"Laboratori Nazionali del Gran Sasso"* (LNGS) [2]. In fact, the ultra-low background at LNGS makes possible to study the nuclear reactions well below the Coulomb barrier [3].

2. Solar neutrinos

Electron neutrinos are produced in the Sun as a product of the nuclear reactions in which four protons are transformed into an α particle, 2 positrons and 2 neutrinos. The hydrogen burning in the Sun is predominantly due to the proton-proton chain (pp chain), while the flux of neutrinos due to the CNO cycle is at the level of 1% [4, 5]. Figure 1 shows the pp chain. About 86% of

http://dx.doi.org/10.1016/j.nuclphysbps.2015.09.291

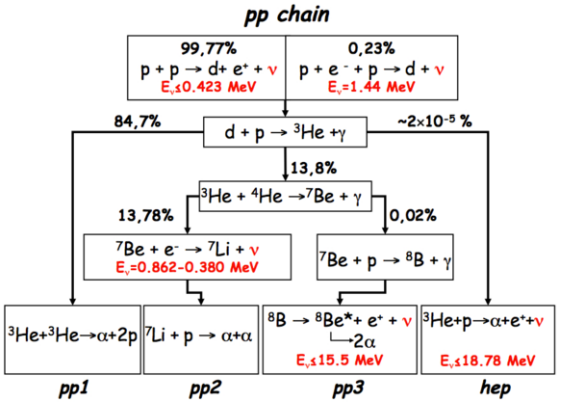

Figure 1: Scheme of the propton-proton reaction chain. The energy production mainly depends on the p-p reaction rate, while the neutrino energy spectrum depends on the competition between successive reactions.

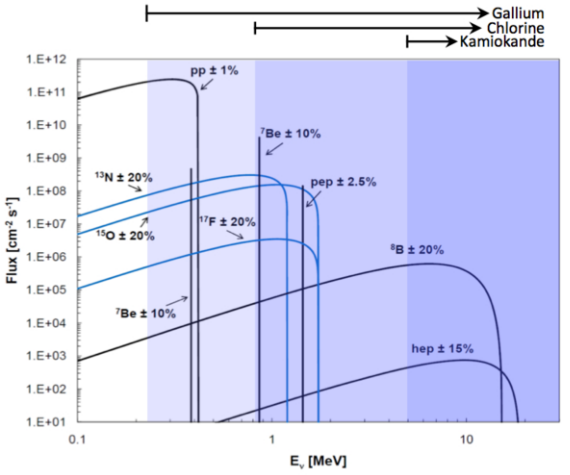

Figure 2: Predicted neutrino flux Vs energy. Also shown are the thresholds of Gallium, Chlorine and Kamiokande experiments.

neutrinos are produced by the $p(p, e^+\nu)D$ reaction (pp neutrinos,$E_\nu \leqslant 0.423\ MeV$). The isotope ^4He is mainly produced by the $^3He(^3He, 2p)^4He$ reaction (pp1 chain, see figure 1). However, a relevant fraction of ^4He (and of neutrinos) is generated through the $^3He(\alpha, \gamma)^7Be$ reaction. The ^7Be can go down two different paths from here. In the pp2 chain the Berililum captures an electron producing mono energetic neutrinos ($E_\nu = 0.370$ and $E_\nu = 0.862\ MeV$, respectively with a Branching ratio of 10% and 90%). This reaction produces 14% of the solar neutrinos. In the pp3 chain the ^7Be reacts with a proton producing ^8B. The ^8B decays into ^8Be producing high energy neutrinos ($E_\nu \leqslant 15.5\ MeV$). This reaction produces about 0.02 % of the solar neutrinos. The subsequent decay of ^8Be produces two α particles. The first observation of solar neutrino was performed by the Davis experiment, in which the detection of ν_e neutrinos was performed with a Chlorine target. The experimental result was a deficit of about a factor 3 with respect to the Standard Solar Model (SSM) results. Afterwards a neutrino deficit was confirmed by the water-Cerenkov Kamioka experiment and by the Gallium experiments (Gallex and Sage). Figure 2 shows the predicted solar neutrino flux as a function of the energy. The figure also shows the experimental threshold of the cited experiments. A long standing solution to explain the solar neutrino deficit was existence of a narrow resonance in the solar Gamow peak region ($15 - 27\ keV$) of the $^3He(^3He, 2p)^4He$ reaction [6, 7]. Such a resonance enhance the rate of the pp1 chain rate, increasing the flux of low energy pp neutrinos and reducing the flux of high energy neutrinos produced in the pp2 and pp3 chains,

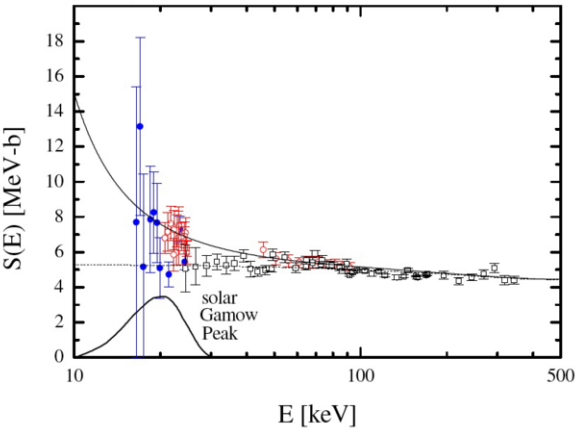

Figure 3: Astrophysical factor of the $^3He(^3He, 2p)^4He$. The LUNA measurements (filled and empty circles) are shown together with previous measurements [8, 9]. The solar Gamow peak region is also shown.

in broadly agreement with the experimental results of the solar neutrino experiments. As a matter of fact, before the LUNA result, the $^3He(^3He, 2p)^4He$ cross section measurements stopped at the center of mass energy of 24.5 keV, leaving the possibility of a narrow resonance inside the solar Gamow peak. In this framework, the LUNA measurement of the $^3He(^3He, 2p)^4He$ inside the solar Gamow peak can be considered a milestone in the long way to the discovery of neutrino oscillation. In fact, for the first time, the astrophysical factor was measured in the whole energy region of interest (the Gamow peak), making much more reliable

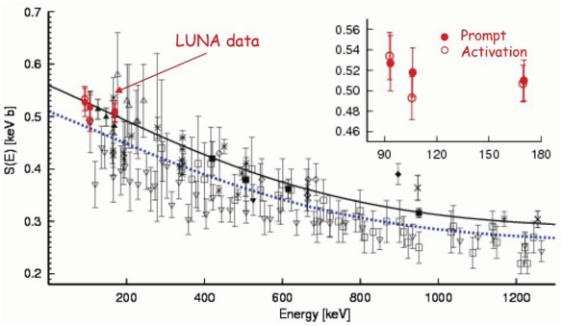

Figure 4: Astrophysical factor of the $^3He(^4He,\gamma)^7Li$. The LUNA measurements (filled and empty circles) are shown together with previous measurements (see [10] and references therein.)

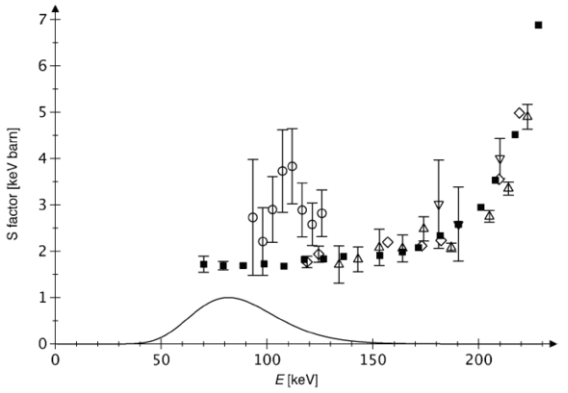

Figure 5: Astrophysical S-factor for the $^{14}N(p,\gamma)^{15}O$. from LUNA data (filled squares) and from previous studies (see [13] and references therein). The Gamow peak for $T_6 = 80\ ^oK$ is also shown.

the calculated solar neutrino luminosity. The LUNA data excluded the existence of a nuclear resonance inside the Solar Gamow peak energy region, therefore a nuclear solution for the *"Solar neutrino problem"* was rejected, pushing towards a new generation of experiments to measure the oscillation parameters and the solar interior (Borexino, Kamland, SNO). Figure 3 shows the data of the astrophysical factor $S(E)$ performed by LUNA. At energy of $E_{cm} = 16.5\ keV$ the cross section is $0.02 \pm 0.02\ pb$, which corresponds to a rate of about 1 event/month, rather low even for the *"silent"* experiments of underground physics [8].

After the discovery of the solar neutrino oscillation, the main goal of the solar neutrino experiments is presently the study of the solar interior. In this concern, the Boron neutrino flux is a *"thermometer"* of the core of the Sun, in fact it is proportional to $T_\odot^{20}$, where $T_\odot$ is the temperature of the core of the Sun. As stated above, the ^8B neutrino flux depends on the accurate knowledge of the reactions $^3He(^4He,\gamma)^7Be$. Before the LUNA measurement, the main source of uncertainty was the difference between direct measurements, where prompt γ rays are detected, and indirect measurements, where the γ's yield from the decay of ^7Be (half-life of 53.22 ± 0.06 days) is measured. Figure 4 shows the astrophysical factor of this reaction measured by LUNA and other experiments. The LUNA data provides at the same time the data at the lowest energy with the best accuracy at the same time, by detecting the yields of prompt and delayed γ's. With this measurement, the uncertainty of the ^8B (^7Be) calculated neutrino flux due to S_{34} has been reduced from 7.5 % (8.0 %) to 2.4 % (2.5 %). The overall uncertainty, including the astrophysical parameters, goes from 12 % (9.4 %) to 10.0 % (5.5 %) [10].

Although the CNO cycle is less effective for the hydrogen burning is the Sun, the neutrinos produced in this way are very important because they are a direct probe to measure the solar metallicity [4]. The measurement of the CNO neutrino flux is therefore one of the main goal of the Borexino experiment, to establish the abundance of *"metals"* in the Sun. The rate of the CNO cycle depends almost linearly by the slowest process of the cycle, the $^{14}N(p,\gamma)^{15}O$ reaction. This reaction has been measured by LUNA in several steps and with different techniques, with the aim of reaching an energy close to the Gamow peak region. The partial cross sections involving the complex ^{15}O level structure, have also been measured at low energy, to obtain a reliable extrapolation of the astrophysical S-factor [11, 12]. The lowest energy reached by LUNA was 70 keV, which corresponds to about 11 $counts/day$, with a cross section of about 0.2 pb [13]. As shown in figure 5, the LUNA measurement establishes that the astrophysical factor, extrapolated at zero energy, is a factor 2 lower with respect to previous estimation. The direct consequence for the SSM is the halving of estimated CNO neutrino flux with respect to previous estimations. It is worth to point out that previous data are in fairly agreement with the LUNA ones; however, the lack of low energy data togheter with the overestimation of the direct transition cross section to the ^{15}O ground state led to a wrong extrapolation in the low energy region.

3. Neutrinos and Big Bang Nucleosynthesis

In the standard cosmology the expansion rate of the universe is governed by the Freidmann equation:

$$H^2 = \frac{8\pi}{3} G\rho \qquad (2)$$

Were H is the Hubble parameter, G is the Newton's gravitational constant and ρ is the energy density which, in the early Universe, is dominated by the *"radiation"*, i.e. the contributions from massless or extremely relativistic particles. The radiation density is often expressed as follows:

$$\rho = \rho_\gamma \left(1 + \frac{7}{8}\left(\frac{4}{11}\right)^{4/3} N_{eff}\right) \quad (3)$$

In this formula ρ_γ is the photon density and N_{eff} is the contribution of other relativistic species. Using this formula $N_{eff} = 3.046$ if only the three known neutrino families are considered.

The figure 6 shows the schematic of BBN chain.

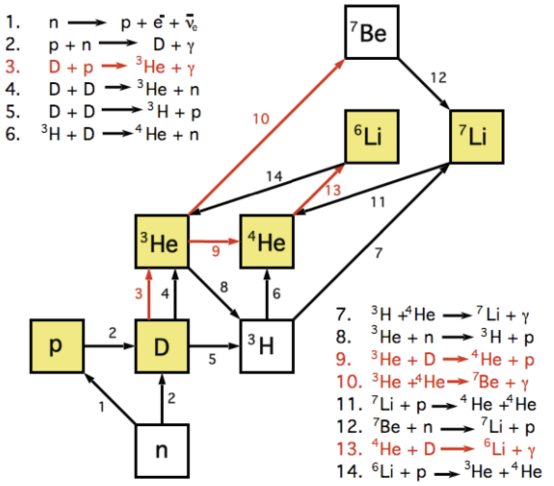

Figure 6: Leading processes of Big Bang Nucleosynthesis. Yellow boxes mark stable isotopes.

Nearly all the free neutrons end up bound in the most stable light element ^4He, whose abundance weakly depends on the cross sections of the BBN processes. Instead, the abundance of the other isotopes strongly depends on the BBN network details and are produced in residual quantities.

Constraints on cosmology and particle physics can be obtained by comparing the calculated abundances provided by the BBN theory with the direct observations of light isotopes in astrophysical objects. Figure 7 shows the abundance of the ^4He primordial mass fraction Y_p and the deuterium abundance D/H as function of the baryon-to-photon ratio baryon density η. In the figure is also shown the result of direct observations and the the dependence of Y_p and D/H on the number of effective neutrino families N_{eff}. The helium abundance

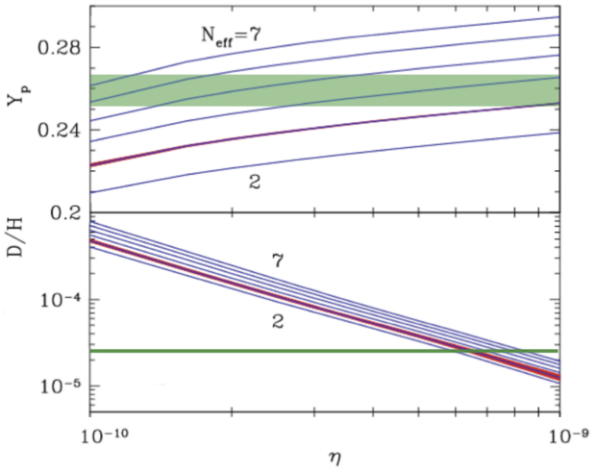

Figure 7: Abundances of helium and deuterium as functions of the baryon-to-photon ratio, η. The blue lines indicate abundances for a single value (integer plus 0.046) of N_{eff}. The red bands indicate the nuclear uncertainty on those yields for $N_{eff} = 3.046$. Also shown are horizontal green bands indicating observational constraints on Y_p and D/H abundances [14, 15].

is very sensitive to N_{eff} while it weakly depends on η. Instead, D/H strongly depends on η, and it is also sensitive to N_{eff}. This two isotopes are indeed useful to infer the baryon density and to constrain the existence of dark radiation. Unfortunately, as shown in figure 7, the Y_p value obtained from astrophysical observations is affected by large systematics because the ^4He abundance is affected by the stellar evolution in a complicated way. The measured abundance of deuterium D/H_{obs} in Damped Lyman-Alpha (DLA) systems at high redshifts has been recently measured with high precision, providing $(D/H)_{obs} = (2.53 \pm 0.04) \times 10^{-5}$ [14]. The theoretical value obtained assuming standard ΛCDM model, the baryon density measured by the PLANCK experiment [16] and using the public BBN code PArthENoPE [17] is $(D/H)_{BBN} = (2.65 \pm 0.07) \times 10^{-5}$ [18]. Interestingly, the theoretical value of D/H is less accurate with respect to the measured one, mainly because of the uncertainties of the BBN nuclear processes responsible for the initial deuterium production and its subsequent processing into $A = 3$ nuclei. The four leading reactions responsible of the deuterium abundance are listed in Table 1 [18]. This table shows that the main source of uncertainty is due to the radiative capture process $D(p,\gamma)^3He$ converting deuterium into ^3He, as a consequence of the lack of data for the $D(p,\gamma)^3He$ reaction in the BBN energy range. Therefore, the forthcoming study at LUNA of the $D(p,\gamma)^3He$ process is of crucial importance to

Table 1: List of the leading reactions and corresponding rate symbols controlling the deuterium abundance after BBN. The last column shows the error on the ratio D/H coming from experimental (or theoretical) uncertainties in the cross section of each reaction, for a fixed baryon density $\Omega_b h^2 = 0.02207$.

Reaction	Rate Symbol	$\sigma_{D/H} \cdot 10^5$
$p(n,\gamma)^2H$	R_1	± 0.002
$d(p,\gamma)^3He$	R_2	± 0.062
$d(d,n)^3He$	R_3	± 0.020
$d(d,p)^3H$	R_4	± 0.0013

improve the uncertainty of deuterium abundance. In the following it will be briefly discussed the importance of this measurement to better constrain the baryon density and the existence of dark radiation.

3.1. Baryon density.

The most recent CMB-derived baryon density is provided by the PLANCK collaboration [16]. Assuming standard ΛCDM model:

$$\Omega_{b,0}(CMB) = (2.205 \pm 0.028)/h^2 \quad (4)$$

In this equation, $\Omega_{b,0}$ is the present day baryon density of the universe and h is the Hubble constant in units of 100 $km\ s^{-1}\mathrm{Mpc}^{-1}$.
The baryon density can be independently inferred by means of standard BBN theory, by comparing the observed deuterium abundance with the abundance obtained with BBN prediction [14]:

$$\Omega_{b,0}(BBN) = (2.202 \pm 0.019 \pm 0.041)/h^2 \quad (5)$$

The error terms in eq. 5 reflect the uncertainties in observed deuterium abundance and BBN calculation [14]. The latter is due to the 3% uncertainty of computed $(D/H)_{BBN}$, that is mainly due to the experimental error of $D(p,\gamma)^3He$ cross section at BBN energies [14, 19]. It is worth to point out that the baryon density obtained by CMB experiments and BBN refer to different universal epoch. therefore the matching of this independent measurements represents an important check for standard cosmology.

3.2. Neutrinos

In cosmology the definition of N_{eff} is the number relativistic species contributing to the radiation density with respect to photons (see eq. 3). For standard cosmology $N_{eff} = 3.046$ and $\xi = 0$, where ξ is the lepton asymmetry [14, 20]. As shown in figure 7, deuterium and helium abundances depend on N_{eff}, therefore it is possible to bound the density of relativistic species by

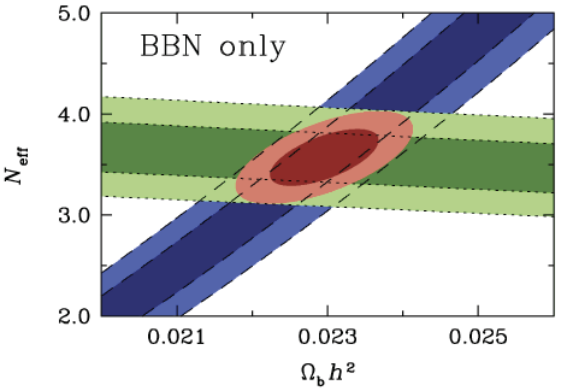

Figure 8: The 1 σ and 2 σ confidence contours (dark and light shades respectively) for N_{eff} and $\Omega_{b,0}$ derived from the primordial deuterium abundance (blue), the primordial He mass fraction (green), and the combined confidence contours (red) [14].

comparing the BBN predictions with observed abundances of D/H and Y_p [14, 19, 20]. the BBN-only bound reported in [14] is:

$$N_{eff}(BBN) = 3.57 \pm 0.18 \quad (6)$$

This constrain is graphically shown in Figure 8, in which the green bands represent the confidence contours related to the helium abundance. The width of the uncertainty is essentially due to the systematics errors of direct observations of Y_p. The blue bands are the confidence contours for deuterium abundance. As stated above (see also eq. 5), this uncertainty is mainly due to the $D(p,\gamma)^3He$ data uncertainty at BBN energies. The CMB-only bound on N_{eff} obtained by the PLANCK experiment is [16]:

$$N_{eff}(CMB) = 3.36 \pm 0.34 \quad (7)$$

It is worthwhile to point out that CMB and BBN constraints are in good agreement and provide a suggestive, but still inconclusive, hint of the presence of dark radiation. A renewed study of the $D(p,\gamma)^3He$ reaction is then mandatory to reduce the N_{eff} uncertainty.

3.3. The deuterium abundance and $D(p,\gamma)^3He$ reaction.

Figure 9 shows the data of the $D(p,\gamma)^3He$ reaction in literature. The precise low-energy data come from the LUNA measurement performed with the 50 kV accelerator [21]. Only a single dataset of S_{12} is currently available in the relevant energy range [22], in which the authors state systematic uncertainty of 9%. Figure 9 also shows behavior of S_{12} as obtained by *"ab initio"*

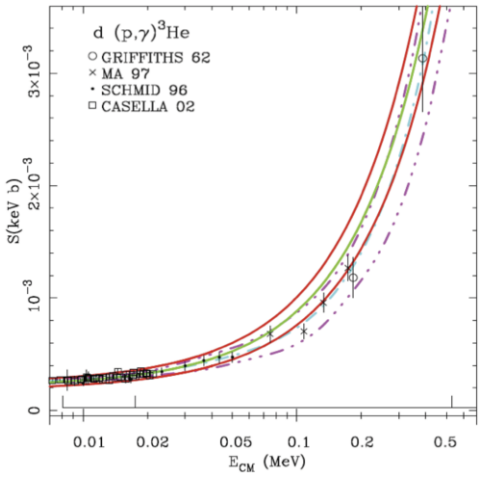

Figure 9: S-factor data for the reaction $D(p,\gamma)^3He$. The best-fit curve (dash-dot curves) and theoretical calculation (solid) are shown. All errors are shown as 2 σs.

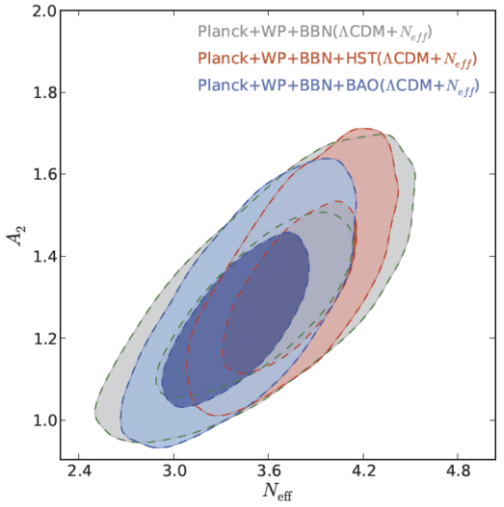

Figure 10: 2-D contour plots in the N_{eff} vs A_2 plane, showing preferred parameter regions at the 68% and 95% confidence levels in the case of the extended ΛCDM model with extra relativistic degrees of freedom [18].

calculation [19, 23, 24]. It is worthwhile to note that the theoretical result is systematically larger than the bestfit value derived from the experimental data in the BBN energy range. The existing difference between theory and data let some author to adopt the theoretical curve (see for example [19]) or the S_{12} value obtained from measurements [16]. Figure 10 shows the 2-D contour plots in the N_{eff} vs A_2 plane, where A_2 is the $D(p,\gamma)^3He$ reaction rate normalized to the value obtained with data fit [18]. Interestingly, the figure 10 favor a $S_{12}(E)$ trend close to the one obtained with *ab initio* calculation, and a N_{eff} value higher than 3 [18]. Therefore, the measurement of $S_{12}(E)$ at BBN energies is of primary importance to understand the origin of the tension between data and *ab initio* calculation for the ^3He isotope, presently with an estimated error of less than 7%.

3.4. The $D(p,\gamma)^3He$ reaction at LUNA

The feasibility of studying the ^2H(p,γ)^{3}He reaction (Q = 5.5 MeV) with good accuracy has been demonstrated at $2.5 < E_{cm}(keV) < 22$ with the previous LUNA 50 kV accelerator (see figure 9) [21]. Figure 11 a) shows the scheme of the setup used in [21], where a barrel BGO detector is implemented. The high efficiency ($\sim$ 70%) of the BGO detector reduces the dependence of the reaction yield due to the angular distribution of the emitted γ rays and thus is a prerequisite to achieve a low systematic uncertainty. The detection efficiency can be determined by precise Monte Carlo simulations, as well as performing dedicated measurements and calibrations, e.g. by measuring the absolute efficiency at a γ ray energy of 6.13 MeV exploiting the 340 keV resonance in the $^{19}F(p,\alpha\gamma)^{16}O$ reaction. With the proposed setup the expected counting rate (full detection γ-peak) is of the order of $10^4 - 10^5$ $events/hour$ in the considered energy range (see figure 12), making the measurements with BGO detector relatively fast for what concern statistics and allowing to determine the beam heating effect and the target density in asymptotical conditions, by performing dedicated measurements in which target pressure and beam intensity are varied. Finally, the beam intensity error can be minimized by a proper calibration of the calorimeter (1.5% uncertainty in ref. [27]). Although the large angular coverage of BGO detector makes the counting yield nearly independent of the angular distribution of emitted photons, an exhaustive study of the $D(p,\gamma)^3He$ reaction includes the study of angular distribution of emitted γ-rays, in order to precisely evaluate the response of BGO detector. This study can be accomplished by using a large high purity Germanium (HPGe) detector facing the gas target in a close geometry, as it is shown in figure 11b), in which the setup already used for the study of the $^2H(\alpha,\gamma)^6$Li reaction is shown [25, 26]. With this setup the angular distribution can be inferred by exploiting the high energy resolution of the detector and the doppler effect affecting the energy of γ's produced along the beam line by the $D(p,\gamma)^3He$ reaction. This study provides an important experimental input for theoretical nuclear physics. In fact, as stated above, the tension between

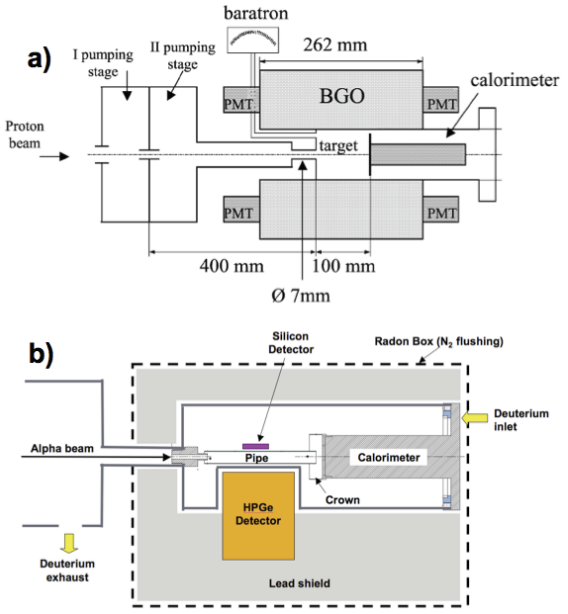

Figure 11: a): Scheme of gas target setup and BGO detector. b): Scheme of gas target setup and HPGe detector.

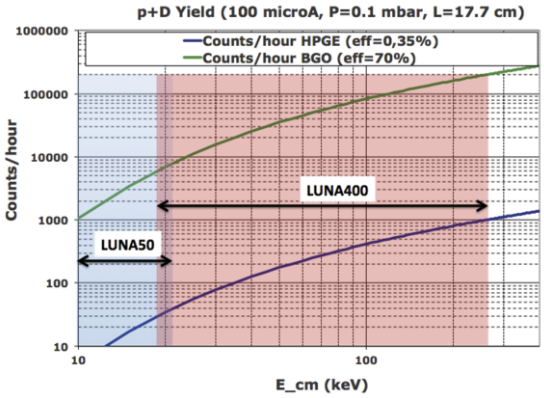

Figure 12: Reaction yields at LUNA400, using the BGO detector (green line, see figure 11a) and the HPGe detector (blue line, see figure 11b). In the figure the working conditions, the energy range of the proposed experiment and of the previous LUNA measurement is also indicated [21].

existing data at BBN energies and *ab initio* calculation is presently debated.

4. Conclusions

In this paper the close interplay between the LUNA measurements and the neutrino physics has been discussed. Several key reactions of the hydrogen burning of the Sun has been studied, providing a decisive improvement of the SSM and consequently to the study of solar neutrino mixing parameters.

The nuclear astrophysics at LUNA is also very important to study the nuclear reactions of the BBN chain. In fact, the progress on direct observations of deuterium abundance [14] and the accuracy of CMB data [16] make the lack of $D(p,\gamma)^3$He reaction data at BBN energies the main obstacle to improve the constraints on $\Omega_{b,0}(BBN)$, N_{eff} and lepton degeneracy ξ [14, 19]. The study of the $D(p,\gamma)^3He$ reaction in the BBN energy range, with an accuracy substantially better with respect the present 9% systematic uncertainty of the S_{12} factor is extremely important in this concern. As light nuclei are involved in this process, the $D(p,\gamma)^3He$ reaction is of high interest also in theoretical nuclear physics. This study will be performed with the LUNA facility at the Gran Sasso laboratory, where the very low environmental background allows to substantially reduce the present data uncertainty.

References

[1] C. Rolfs and W .S. Rodney, Cauldrons in the Cosmos (University of Chicago press, 1988).
[2] A. Formicola *et al*, Nucl. Instr. and Meth. A **507** 609 (2003).
[3] A. Caciolli *et al*, Eur. Phys. J. A **39**, 179 (2009).
[4] J.N. Bahcall, M.H. Pinsonneault, Rev. Mod. Phys. **64**, 885 (1992).
[5] A.M. Serenelli, Proc. of the XIV Int. Workshop on "Neutrino Telescopes", Venice, Italy (20122). arXiv:1109.2602.
[6] W.A. Fowler, Nature **238**, 24 (1972).
[7] V.N. Fetysov and Y.S. Kopysov, Phys. Lett. B **40**, 602 (1972).
[8] R. Bonetti *et al*, Phys. Rev. Lett. **82**, 5205 (1999).
[9] A. Krauss *et al*, Nucl. Phys. A **467**, 273 (1987).
[10] F. Confortola *et al*, Phys. Rev. C **75**, 065803 (2007).
[11] A. Formicola *et al*, Phys. Lett. B **591**, 61 (2004).
[12] M. Marta *et al*, Phys. Rev. C 78, 022802 (2008).
[13] A. Lemut *et al*, Phys. Lett. B **634** 483 (2006).
[14] R. Cooke *et al*, ApJ. **781**, 31, (2014).
[15] Y.I Izotov, G. Stasinska, N.G. Guseva: AA **558**, A57 (2013).
[16] PLANCK collaboration: arXiv:1303.5076v1 [astro-ph.CO] (2013).
[17] O. Pisanti *et al*, Comput. Phys. Commun. 178, 956 (2008).
[18] E. Di Valentino *et al*, Phys. Rev. D **90**, 023543 (2014).
[19] K.M. Nollett and G.P. Holder: arXiv:1112.2683v1 [astro-ph.CO] 12 Dec 2011.
[20] G. Steigman: Adv.High Energy Phys. 2012 (2012) 268321.arXiv:1208.0032v1 [hep-ph] 31 Jul 2012.
[21] C. Casella *et al*, Nuclear Physics A **706** 203216. (2002).
[22] L. Ma *et al*, Phys. Rev. C **55**, 588 (1997).
[23] M. Viviani *et al*, Phys. Rev. C **61**, 064001 (2000).
[24] L. E. Marcucci *et al*, Phys. Rev. C **72**, 014001 (2005).
[25] H. Costantini *et al*, Nuclear Physics A **814** 144158 (2008).
[26] M. Anders *et al*, Eur. Phys. J. A **49** 28 (2013).
[27] M. Anders *et al*, PRL **113**, 042501 (2014).